Journal of Physics: Conference Series **640** (2015) 012010 doi:10.1088/1742-6596/640/1/012010

Kinetics of directed self-assembly of block copolymers on chemically patterned substrates

Marcus Müller, Weihua Li, Juan Carlos Orozco Rey, and Ulrich Welling

Institute for Theoretical Physics, Georg-August University, D37073 Göttingen, Germany

E-mail: mmueller@theorie.physik.uni-goettingen.de

Abstract. Chemically patterned surfaces have been successfully employed to direct the kinetics of self-assembly of block copolymers into dense, periodic morphologies ("chemoepitaxy"). Significant efforts have been directed towards understanding the kinetics of structure formation and, particularly, the formation and annihilation of defects. In the present manuscript we use computer simulations of a soft, coarse-grained polymer model to study the kinetics of structure formation of lamellar-forming block copolymer thin films on a chemical pattern of lines and spaces. The case where the copolymer material replicates the surface pattern and the more subtle scenario of sparse guiding patterns are considered. Our simulation results highlight (1) the importance of the early stages of pattern-directed self-assembly that template the subsequent morphology and (2) the dependence of the free-energy landscape on the incompatibility between the two blocks of the copolymer.

1. Introduction

Block copolymers are comprised of two or multiple blocks of chemically distinct repeat units joined by covalent bonds into a flexible macromolecule. By virtue to the small translational entropy, a minuscule repulsion between unlike blocks gives rise to phase separation. The connectivity of the blocks along the chain molecule prevents the formation of macroscopically extended domains. Instead the different blocks form spatially modulated structures. The symmetry and connectivity of these microphase-separated structures can be controlled by the macromolecular architecture, i.e., the volume fraction f of the blocks, their spatial extension, and their incompatibility, χN [1]. The characteristic spatial dimension of the microphase-separated structure is dictated by the end-to-end distance R_{e0} of the molecules, and it is of the order of 1-100 nanometers [2]. Therefore, these polymeric materials have attracted abiding interest for templating nanostructures in the context of filtration, catalysis, or microelectronic device manufacturing [3, 4].

The latter application exploits a combination of extreme UV lithography and block copolymer self-assembly ("block copolymer lithography" [3, 5, 6, 7]). Extreme UV lithography is employed to fabricate a chemical guiding pattern. In the following we restrict ourselves to a pattern of lines and spaces (L/S). This chemical guiding pattern directs the self-assembly ("directed self-assembly/DSA") of symmetric, lamella-forming AB diblock copolymer in a thin film on top of the chemical L/S guiding pattern. If the lines and spaces of the L/S guiding pattern coincide with the period L_0 of the lamellar structure of the block copolymers in the bulk and if both blocks have similar affinity to the free surface of the film, the copolymer will replicate the L/S guiding

pattern and form standing lamellae orientated perpendicular to the film surfaces [8, 9, 10]. The stripe structure of the block copolymer mitigates the line-edge roughness [11, 12] or small imperfections of the guiding pattern. Alternatively the periodicity of the L/S guiding pattern can be a small multiple of the bulk lamellar structure of the copolymer ("density multiplication" [13, 14, 15]). In this case the copolymer structure will "fill-in" the missing lines and multiply the density of the L/S guiding pattern fabricating a pattern with periodicity of a few tens of nanometers.

Defects in block copolymer lithography refer to localized structures of the copolymer material that deviate from the ideal L/S pattern [16]. The types of defects that are observed in experiments encompass *inter alia* broken lines or spaces ("micro-bridges"), dislocations and disclinations. The integration of block copolymer lithography into microelectronic device manufacturing poses extreme demands of the areal density of defects – industry standards require that the DSA should result in less than 0.01 defect per square centimeter [17]!

Thermodynamically, such a strict requirement can be fulfilled because the excess free energy ΔF_d of a defect exceeds the thermal energy scale $k_\mathrm{B}T$ by about two orders of magnitude [18]. This large defect free energy can be rationalized as follows: Since a macromolecule in a polymer melt adopts a fractal, random-walk-like conformation, ${R_\mathrm{e0}}^2 = b^2(N-1)$ where b and N denote the statistical segment length and number of segments, respectively, one molecule interacts with many neighbors. The number of interaction partners, $\sqrt{\bar{N}} \equiv \rho {R_\mathrm{e0}}^3/N \sim \sqrt{N}$ (ρ being the number density of segments), typically adopts large values of the order 10^2, and the free-energy scale is set by $k_\mathrm{B}T\sqrt{\bar{N}}$. Locally the distortion of the internal AB interfaces resembles a grain boundary and the typical grain-boundary free energy scales like $\gamma_\mathrm{gb} \sim 0.1 k_\mathrm{B}T\sqrt{\bar{N}}/{R_\mathrm{e0}}^2$ [19, 20] and the typical defect area is of the order of a few lamellar spacings L_0 times the film thickness $D \sim L_0$. The concomitant defect density scales like $\sigma_\mathrm{d} \sim \exp(-\Delta F_\mathrm{d}/k_\mathrm{B}T)/L_0^2 \sim 0.001/\mathrm{cm}^2$ for $\Delta F_\mathrm{d} = 30 k_\mathrm{B}T$.

Nevertheless, the fact that a significantly higher defect density has been observed in DSA experiments demonstrates that defects cannot be conceived as equilibrium fluctuations around a perfectly ordered structure [18, 21]. Instead, defects are rather metastable localized structures, into which the system got trapped in the course of structure formation. Therefore it is important to understand and control the kinetics of self-assembly and defect-annihilation mechanisms in the DSA of block copolymer materials. This is a computational challenge because (1) structure formation evolves on the time scale of minutes or hours that are inaccessible to atomistic modeling and (2) the free-energy landscape, which provides a basic ingredient for the understanding of the adiabatic structure formation, is complex.

In this manuscript we use a soft, coarse-grained polymer model [22, 23] that is able to describe the kinetics of structure formation on the pertinent time and length scales. Then we discuss the kinetics of structure formation for pattern replication, i.e., when there is a one-to-one correspondence between the chemical guiding pattern and copolymer structure, and for two-fold density multiplication. We highlight the role of the guiding pattern at the initial stage of self-assembly and the dependence of the free-energy landscape on incompatibility. The manuscript closes with a brief summary and discussion.

2. Model and simulation technique

The large time and length scales – minutes and micrometer – require the use of highly coarse-grained models, in which a single interaction center (segment) represents several tens of monomeric repeat units of a chemically realistic description. On the length scale of such a highly coarse-grained segment, the macromolecule already adopts its random-walk like statistics and the distances are Gaussian distributed. Therefore we use a discretized Edwards Hamiltonian

to model the connectivity along the polymer backbone [22, 24, 23]

$$\frac{\mathcal{H}_{\mathrm{b}}}{k_{\mathrm{B}}T} = \sum_{i=1}^{N} \frac{3(N-1)}{2{R_{\mathrm{e0}}}^2} \sum_{s=1}^{N-1} \left[\mathbf{r}_i(s+1) - \mathbf{r}_i(s)\right]^2 \tag{1}$$

where the first sum, $i = 1, \cdots, n$ runs over all diblock copolymers that are comprised of $N = 32$ segments. $\mathbf{r}_i(s)$ denotes the spatial position of the s^{th} segment of polymer i. The molecular density is $\sqrt{\bar{N}} = 128$ in all following simulations.

Since each coarse-grained segment corresponds to a multitude of monomeric repeat units, their center-of-mass positions may overlap without violating the excluded volume condition for the atomistic constituents. Therefore we describe the non-bonded interactions between coarse-grained segments by soft potentials. The non-bonded interactions represent two relevant interactions: (1) the low compressibility of a dense polymer liquid that stems from the excluded volume of the constituent atoms and (2) the repulsion between A and B segments that gives rise to microphase separation.

$$\frac{\mathcal{H}_{\mathrm{nb}}}{k_{\mathrm{B}}T\sqrt{\bar{N}}} = \int \frac{\mathrm{d}^3\mathbf{r}}{{R_{\mathrm{e0}}}^3} \left\{ \frac{\kappa N}{2} \left[\hat{\phi}_A(\mathbf{r}|\{\mathbf{r}\}) + \hat{\phi}_B(\mathbf{r}|\{\mathbf{r}\}) - 1\right]^2 - \frac{\chi N}{4} \left[\hat{\phi}_A(\mathbf{r}|\{\mathbf{r}\}) - \hat{\phi}_B(\mathbf{r}|\{\mathbf{r}\})\right]^2 \right\} \tag{2}$$

where $\kappa N = 50$ is the dimensionless inverse isothermal compressibility of the dense liquid, and χN denotes the product of Flory-Huggins parameter and number of segments per polymer that parameterizes the incompatibility of the distinct blocks. $\hat{\phi}_A(\mathbf{r}|\{\mathbf{r}\})$ denotes the local volume fraction of A segments that depends on the microscopic configuration $\{\mathbf{r}\}$.

$$\hat{\phi}_A(\mathbf{r}|\{\mathbf{r}\}) = \frac{1}{\rho} \sum_{i=1}^{n} \sum_{s=1}^{fN} \delta(\mathbf{r} - \mathbf{r}_i(s)) \tag{3}$$

where $f = 1/2$ is the fraction of A segments. A similar expression holds for the dimensionless B density. In order to numerically evaluate the density, Eq. (3), and the integral in Eq. (2) we use a collocation grid with spacing $\Delta L \approx R_{\mathrm{e0}}/6$ and use a linear assignment of the particles to the mesh. Measuring the anisotropy of the bonded stress parallel and perpendicular to the lamellae we identified the equilibrium lamellar spacing, L_0, in the bulk yielding $L_0 = 1.68R_{\mathrm{e0}}$ and $1.58R_{\mathrm{e0}}$ for $\chi N = 30$ and 20, respectively.

We consider a thin film with geometry $D \times L_y \times L_z$. Periodic boundary positions are applied in the two lateral directions y and z. The confining substrate at $x = 0$ and the air/vacuum surface at $x = D$ are represented by hard, impenetrable walls. This is a good approximation because the surface tension of the polymer with air is about an order of magnitude larger than the tension of the internal AB interfaces and, consequently, there is hardly any deformation of the free surface of the polymer film for standing lamellae. Moreover, the limitation of our highly coarse-grained model in representing the narrow polymer-substrate and polymer/air interfaces does not warrant a more detailed modeling of the film surfaces [25].

We represent the chemical guiding pattern by a short-range potential [26]

$$\frac{\mathcal{H}_{\mathrm{s}}}{k_{\mathrm{B}}T\sqrt{\bar{N}}} = -\frac{\Lambda N R_{\mathrm{e0}}}{\epsilon} \int \frac{\mathrm{d}^3\mathbf{r}}{{R_{\mathrm{e0}}}^3}\, e^{-\frac{x^2}{2\epsilon^2}} f_{\mathrm{s}}(y,z) \left[\hat{\phi}_A(\mathbf{r}|\{\mathbf{r}\}) - \hat{\phi}_B(\mathbf{r}|\{\mathbf{r}\})\right] \tag{4}$$

where f_{s} adopts the value $+1$ on A-attracting lines of the guiding pattern, 0 on neutral patches of the substrate, and negative values on B-attractive areas. $\epsilon = 0.15R_{\mathrm{e0}}$ characterizes the perpendicular range of the surface potential and ΛN denotes its selectivity. Since the two blocks of the copolymer are structurally symmetric, they suffer the same entropy loss at the substrate,

and we can approximate the surface free energy difference, $\Delta\gamma$, of the two components by the surface energy difference [27]

$$\frac{\Delta\gamma {R_{e0}}^2}{k_B T\sqrt{\bar{\mathcal{N}}}} \approx \sqrt{2\pi}\Lambda N \tag{5}$$

The top surface to air/vacuum is non-preferential in all simulations.

We use Smart Monte-Carlo (SMC) updates [28] in conjunction with the Single-Chain-in-Mean-Field algorithm [29]. The former scheme biases the proposed, local, random displacements of coarse-grained segments according to the strong bonded forces. In conjunction with the soft, non-bonded interactions it results in Rouse-like dynamics [30, 31]. From the single-chain diffusion coefficient D_{diff} we obtain a characteristic time $\tau = {R_{e0}}^2/D_{\text{diff}} = 8990$ SMC moves per segment. The Single-Chain-in-Mean-Field algorithm is the Monte-Carlo analog of multiple-time step algorithm in molecular dynamics simulations [32] and temporarily replaces the weak, non-bonded forces by external, fluctuating fields that are recomputed from the instantaneous microscopic densities, Eq. (3), after each SMC sweep over all segments [22, 29, 33]. This quasi-instantaneous approximation of the pairwise interactions is accurate and quantitatively describes composition fluctuations. Since the molecular conformations are independently updated, our algorithm is well suited for parallel computations. Taking generic values for molten polymers, $D_{\text{diff}} \approx 10\text{nm}^2/\text{s}$ and $R_{e0} \approx 20\text{nm}$, we obtain an order-of-magnitude estimate $\tau \approx 40\text{s}$. Typically simulations last for $10^5 - 10^6$ SMC corresponding to minutes or hours, respectively. The lateral spatial extensions of our system are $L_y \sim L_z \approx 10L_0 \approx 0.3\mu\text{m}$, and our systems are comprised of more than 10^6 coarse-grained segments.

The model and simulation technique provides a computationally efficient and realistic description of single-chain dynamics and collective kinetics of structure formation of dense multi-component polymer melts of low and intermediate molecular weight. The particle dynamics duly accounts for the coupling between molecular conformations, single-chain dynamics and the kinetics of the collective density that is difficult to accomplish in field-theoretic models. Entanglement effects due to the non-crossability of the chain molecules, strong disparities in the segmental mobilities, or hydrodynamic flow, however, are not captured by our simulation technique. The former effects are only thought to be important for large molecular weights or systems with very disparate glass transition temperatures, or at the late stages of structure formation, respectively.

3. Results

In DSA experiments a mixture of block copolymer and low-molecular-weight co-solvent is spin-coated on the patterned substrate and subsequently annealed at elevated temperature. As the solvent evaporates the polymer concentration increases and structure formation begins. Unfortunately, we lack detailed knowledge about the initial state of structure formation within the first $\tau \approx 40\text{s}$. Therefore we crudely represent the experimental procedure by instantaneously quenching a disordered structure, $\chi N = 0$, to the final value of the incompatibility $\chi N = 30$

The structure formation after this quench can be divided into qualitatively distinct stages:

(i) *initial surface-directed spinodal self-assembly:* The initial kinetics of collective density fluctuations can be qualitatively described by the dynamic Random-Phase Approximation (RPA) [34]. Since the composition is conserved it follows diffusive Cahn-Hilliard dynamics [35, 36]. In Fourier space the time evolution of the local A-density takes the form

$$\frac{\partial\phi_A(\mathbf{q},t)}{\partial t} = -q^2\Lambda(q)\mu(q) \tag{6}$$

where $\Lambda(q) \sim {R_{e0}}^2 g_0(q)/\tau$ denotes the wave-vector-dependent Onsager coefficient and the Debye function, $g_0(q)$, characterizes the Gaussian chain structure [37, 38]. The chemical

potential μ is comprised of two contributions. The first, bulk contribution is proportional to $S(q)\phi_A(\mathbf{q},t)$, where $S(q)$ is the RPA structure factor at $\chi N = 30$. Since the homogeneous structure is absolutely unstable, $S(q)$ is negative in an interval of wave vectors, resulting in an exponential growth of the concomitant Fourier modes of composition fluctuations ("spinodal self-assembly"). The initial amplitude of composition fluctuations, however, is rather small because the large molecular density, $\sqrt{\bar{N}}$, strongly suppresses composition fluctuations in the initial state. The second contribution to μ arises from the chemical guiding pattern, and it is proportional to the Fourier transform, $h(\mathbf{q})$, of the surface potential $\exp(-\frac{x^2}{2\epsilon^2})f_{\rm s}(y,z)$. It gives rise to a linear growth of composition fluctuations with time [39]. In this way the chemical guiding pattern directs the structure formation in the initial stage. [1]

After a time of order τ, one observes the formation of well-segregated domains, inside of which the local densities of A and B segments adopt their saturation values 0 or 1. At the end of the first stage, the overall structure of the copolymer melt is roughly aligned and registered with the guiding pattern but there may be numerous defects.

(ii) *Local defect annihilation and grain formation:* The second stage of structure formation consists in the removal of defects. Defects interact through their distortion of the internal AB interfaces away from the perfectly ordered lamellar structure. These long-range strain fields result in the movement of defects. For instance, dislocations with opposite Burgers vectors attract each other and collide [40, 41, 42]. Upon collision they either annihilate each other or they form a tightly bound, metastable dislocation pair. These metastable defects have a protracted lifetime because the free-energy barrier, $\Delta F_{\rm b}$, which has to be overcome in order to remove the metastable defect, scales like $\sqrt{\bar{N}}k_{\rm B}T$. After the local removal of defects, grains of perfectly ordered regions form. This local defect annihilation completes the DSA process because the chemical guiding pattern registers and aligns the grains with the guiding pattern.

(iii) *Grain coarsening:* In the absence of a guiding pattern, grains are characterized by different orientations and meet at grain boundaries. In that case, there exists a third regime, where the grain structure coarsens by the motion of grain boundaries giving rise to universal power-law behaviour of grain growth [43, 44].

Since we are chiefly interested in the kinetics of DSA we focus on the two initial stages of structure formation in the following.

3.1. Pattern replication

First we study the structure formation of a symmetric diblock copolymer on a L/S pattern whose periodicity exactly matches that of the block copolymer in the bulk at $\chi N = 30$. We use the film thickness $D = \frac{3}{4}L_0 = 1.26R_{\rm e0}$ to maximally frustrate lying lamellae (sandwich structures).

Top-down snapshots and averaged two-dimensional xz density profiles of the copolymer structure at various times are depicted in Figs. 1 and 2. In accord with previous experiments and simulations [9] and the rationale of the previous section, we observe that the guiding pattern rapidly attracts the corresponding blocks and directs the structure formation into a perfectly ordered and registered structure at the chemically patterned substrate within $t = 1000$ SMC

[1] Alternative one could assume that the initial state of structure formation consisted in a solvent-swollen compatible system, $\chi N = 0$, subjected to the interaction with the chemical guiding pattern. In this scenario, the chemical guiding pattern would impose density fluctuations of the form $\phi_A(\mathbf{q}, t = 0) \sim h(\mathbf{q})/S_0(q)$ where S_0 is the structure factor of the disordered system at $\chi N = 0$. These initial density fluctuations would be amplified by the spontaneous structure formation and result in a similar structure evolution, $\phi_A(\mathbf{q},t) - \phi_A(\mathbf{q}, t = 0) \sim q^2 g_0(q) h(\mathbf{q}) t$ during the initial stage (neglecting the wave-vector dependence of the structure factor around its extremum). For selected examples we have verified that this alternative starting configuration yields very similar results.

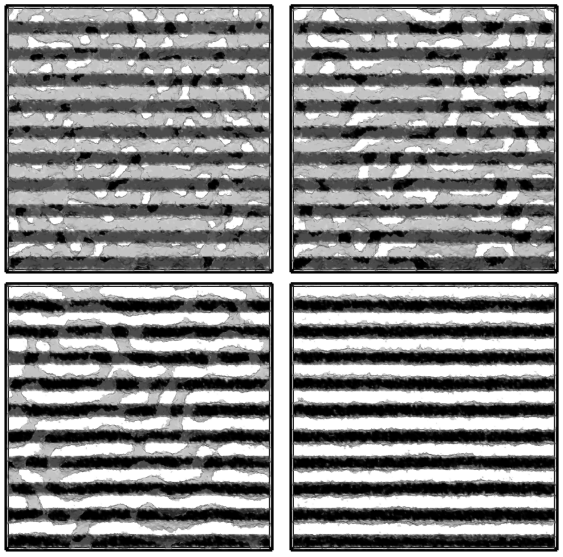

Figure 1. Top-down images of the ordering on a symmetric L/S guiding pattern at $\chi N = 30$. The lateral dimensions are $L_y = L_z = 10L_0$ and the guiding pattern consists of alternating A and B-attractive lines of widths $W/L_0 = 1/2$ and strength $\Lambda N = 2$. The different panels present snapshots at times $t = 1000, 3000, 8000$, and 14000 SMC.

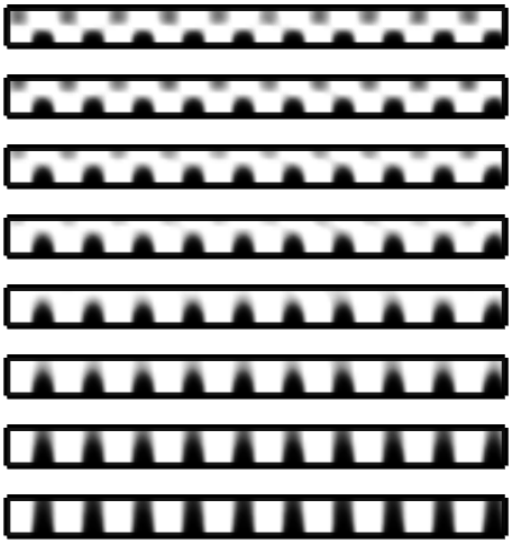

Figure 2. Two-dimensional density profiles for the same system as in Fig. 1 obtained by averaging along the L/S pattern and over 10 independent simulations. The panels correspond to times $t = 1000, 2000, 3000, 4000, 5000, 6000, 8000,$ and 10000 SMC from top to bottom.

$\approx 0.1\tau$. The enrichment of A segments on top of the A-attracting guiding lines gives rise to a concomitant depletion of A segments further away from the substrate. In the averaged side views this checkerboard structure is clearly visible. It consists of a perfectly ordered and registered lamellar grain at the substrate and a top grain that is shifted by half a lamellar period and contains some defects. The perfectly ordered bottom grain and the misaligned top grain are separated by a horizontal grain boundary. From the side views we observe that this horizontal grain boundary gradually moves upwards, i.e., the perfectly ordered bottom grain growths in thickness whereas the misaligned top grain becomes thinner. This process can be conceived as the wetting of the perfectly ordered and registered bottom grain on the chemically guiding pattern. Note that the strength of the chemical guiding pattern is large. The surface free-energy difference $\Delta\gamma$ in Eq. 5 is much larger than the tension of the internal AB interface, $\gamma_{AB}{R_{\mathrm{e}0}}^2/k_{\mathrm{B}}T\sqrt{\mathcal{N}} \approx \sqrt{\chi N/6}$ and therefore even the liquid of segments will wet the corresponding lines of the chemical pattern. The grain boundary tension typically adopts much smaller values [19, 20]. Eventually the misaligned top grain becomes so thin that the shifted stripes break up into spots [9], and defect-free standing lamellae are established at $t = 14000$ SMC $\approx 1.1\tau$.

This initial spontaneous self-assembly is directed by the guiding pattern. During this ideal pattern replication no long-lived metastable defects are formed, and the entire process illustrates the first stage of DSA – surface-directed spinodal self-assembly.

3.2. Density multiplication

Instead of merely replicating (and improving) the guiding pattern, sparse guiding patterns have been successfully used to produce structures with a smaller characteristic dimension than the

guiding pattern [13]. In this second example we study the same system as before but the guiding pattern comprises only 5 A-attracting lines with width $W/L_0 = 1/2$ and a period of $2L_0$, i.e., the line density of the guiding pattern is half than that of the copolymer structure in the bulk. The strength of the A-attracting lines is $\Lambda_s N = 2$ and the substrate area between the lines ("background") does not exhibit any preference for the segment species, $\Lambda_b N = 0$.

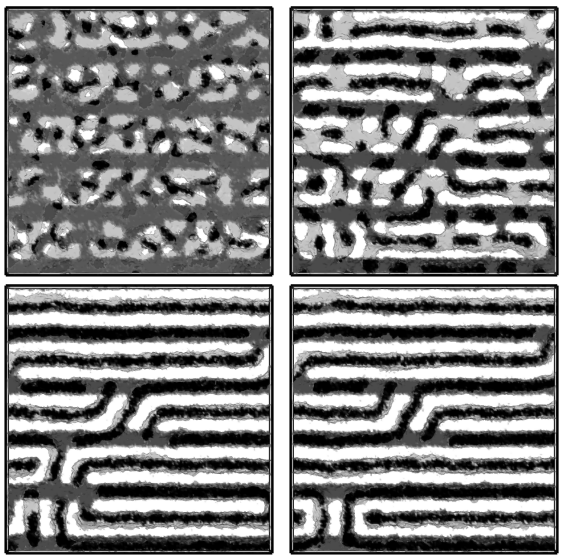

Figure 3. Top-down images of the ordering on a L/S guiding pattern with 2×density multiplication at $\chi N = 30$. The guiding pattern consists of A-attractive lines with $W/L_0 = 1/2$ and $\Lambda N = 2$ on a neutral background. The different panels present snapshots at times $t = 1000, 10000, 100000,$ and $2 \cdot 10^6$ SMC.

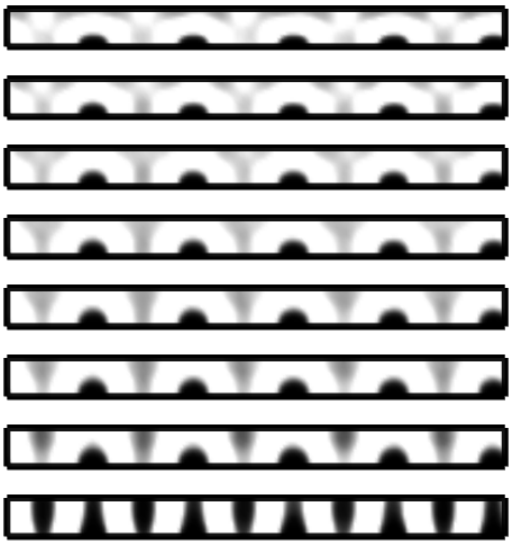

Figure 4. Two-dimensional density profiles for the same system as in Fig. 3 obtained by averaging along the L/S pattern and over 10 independent simulations. The panels correspond to times $t = 1000, 2000, 3000, 4000, 5000, 6000, 10000,$ and 100000 SMC from top to bottom.

The kinetics of structure formation is presented in Figs. 3 and 4. The guiding pattern directs the initial spinodal self-assembly. Within 1000 SMC a thin A-domain is established on top of the A-attracting guiding line and the diffusion of A segments towards the lines gives rise to a cylindrical depletion zone that is clearly visible in Fig. 4. Within a molecular relaxation time, τ, a thin, defect-free and registered A-domain is formed on each A-attracting guiding line, and a preference for additional, standing A-lamellae is established *on average* in the middle between the guiding lines.

In the subsequent course of structure formation the thickness of the defect-free and registered A-domains on the A-attracting guiding line increases and standing A-lamellae are established. On the neutral background, however, the lamellae are riddled with defects forming multiple bridges to the neighboring A-lamellae on top of the guiding lines. Upon annealing, the defect density decreases but some defects are persistent. At $t = 300000$ SMC $\approx 33\tau$ none of the 10 independent systems formed a defect-free lamellar structure. We annealed two systems for up to $2 \cdot 10^6$ SMC $\approx 222\tau$ (see also Fig. 8) but tight dislocation pairs and small dislocations remained (cf. last panel of Fig. 3). This observation provides a clear evidence that these defect structures are metastable and that the thermally activated defect-removal process entails a large free-energy barrier, ΔF_b. This is in good agreement with recent self-consistent field calculations studying the minimum free-energy path of defect removal [21].

The equilibrium properties of copolymers on sparse guiding patterns have been carefully investigated by Detcheverry *et al* [14] and Ramirez-Hernandez and co-workers [15]. Efficiently equilibrating the structures by a sophisticated variety of Monte-Carlo moves – single-bead displacements, reptation, whole-chain translation, and swapping of the two blocks – they observed that a weakly B-attractive background increases the stability of defect-free standing lamellae in comparison to alternate structures, and this finding has been corroborated by experiments [14, 15].

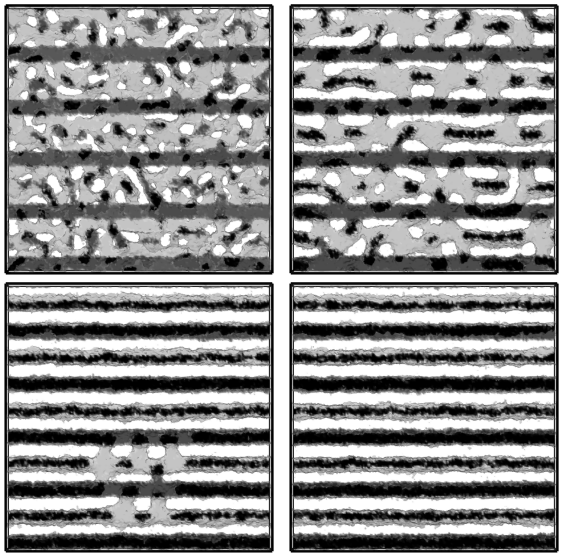

Figure 5. Top-down images of the ordering on a L/S guiding pattern with 2×density multiplication at $\chi N = 30$. The guiding pattern consists of A-attractive lines with $W/L_0 = 1/2$ and $\Lambda N = 2$ on a weakly B-attractive background, $\Lambda_s N = -0.2$. The different panels present snapshots at times $t = 1000, 10000, 100000$, and 200000 SMC.

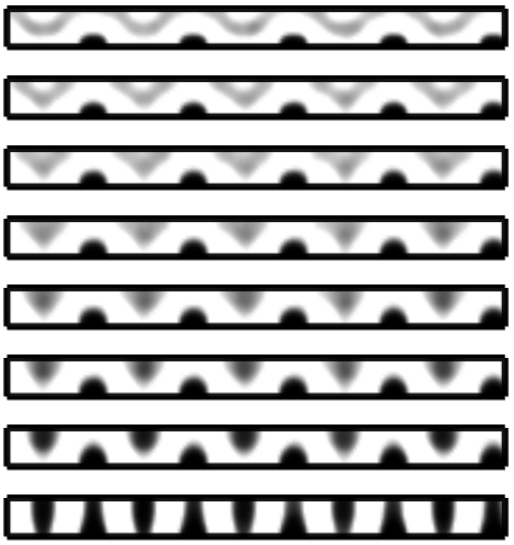

Figure 6. Two-dimensional density profiles for the same system as in Fig. 5 obtained by averaging along the L/S pattern and over 10 independent simulations. The panels correspond to times $t = 1000, 2000, 3000, 4000, 5000, 6000, 10000$, and 100000 SMC from top to bottom.

In Figs. 5 and 6 we present the kinetics of structure formation on a weakly B-attractive background, $\Lambda_b N = -0.2$. Qualitatively the structure formation proceeds similar to the situation with a neutral background. However, the averaged side views in Fig. 6 reveal that at the end of the surface-directed spinodal self-assembly, $t = 10000$ SMC $\approx 1.1\tau$, the copolymer structure is significantly more symmetric. There is an A-domain on top of the strongly A-attractive guiding lines and a similar A-domain at the top of film between the guiding lines (instead of a weak preference for a standing A-lamella for $\Lambda_s N = 0$). This more symmetric averaged structure is less prone to form persistent defects. Typically, defects consists in localized connections between neighboring lines ("micro-bridges", cf. penultimate panel of Fig. 5) that rather rapidly anneal. 7 out of 10 independent simulations achieved defect-free assembly at $t = 200000$ SMC $\approx 22\tau$. The remaining 3 systems featured (i) a micro-bridge, (ii) a partially formed dislocation dipole (see Fig. 7), and (iii) a tight dislocation pair (similar to Fig. 8). The system (i) with the micro-bridge converted into a defect-free structure at time $t = 220000$ SMC, whereas the system (iii) with the tight dislocation pair still retained the defect at $t = 575000$ SMC.

The defect annihilation pathway of the system (ii) with a partial dislocation dipole is

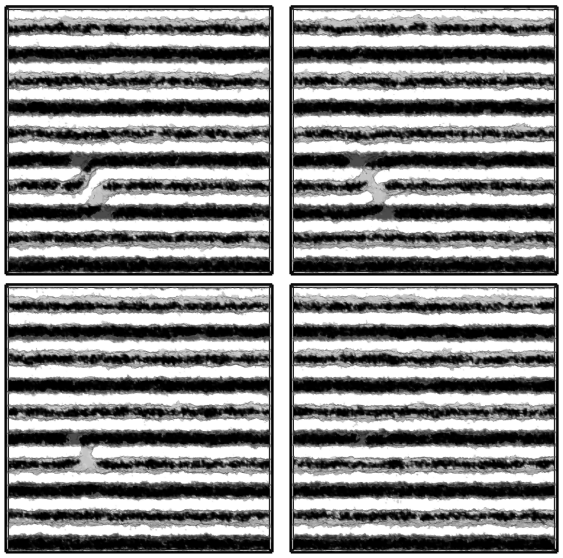

Figure 7. Top-down images of the annihilation of a partially formed dislocation dipole on a L/S guiding pattern with 2×density multiplication (same system as in Fig. 5). The top-down images illustrate the sequence of structures along the pathway of defect annihilation. The panels correspond to times $t = 200000, 388000, 398000$, and 404000 SMC.

illustrated in Fig. 7. At $t = 200000$ SMC there is a dislocation dipole but the lower one of the two A-connections between the A-lamella on the A-attractive line of the guiding pattern and the A-stripe on the weakly B-attractive background is broken at the bottom substrate. Although the dislocation dipole is only partially formed it is quite persistent. At time $t = 388000$ SMC, however, the two ends of the A-stripe on the weakly B-attractive background join at the neutral top surface, and the second, upper A-connection that bridges across the weakly B-attractive background is broken at the bottom substrate. Subsequently, at $t = 398000$ SMC, the lower A-connection vanishes completely and, finally, at $t = 404000$ SMC the defect-free lamellar structure is established. This sequential pathway of defect removal, which we observe in our dynamic particle simulations, is very good agreement with our results on defect annihilation mechanisms using the string method in conjunction with self-consistent field theory [21].

3.3. Process-directed self-assembly

Our self-consistent field theory study of defect annihilation mechanisms in thin films of lamella-forming diblock copolymers [21] demonstrated that there exists an interval of incompatibilities, $\chi_{\mathrm{ODT}}N \approx 10.5 < \chi N < \chi N_*$, between the order-disorder transition (ODT) and a threshold χN_* where two conditions are met: (1) The excess free energy of a defect is large compared to the thermal energy scale, $\Delta F_{\mathrm{d}} \gg k_{\mathrm{B}}T$, and consequently defects are not spontaneously generated in a defect-free structure by thermal fluctuations and (2) the free-energy barrier ΔF_{b} for defect annihilation is comparable to $k_{\mathrm{B}}T$ and thus defects are not even metastable but spontaneously annihilate. This interval of incompatibility in the vicinity of the order-disorder transition is very favorable for defect-free directed self-assembly. In the absence of a guiding pattern, the minimum free-energy path calculations predict $\chi N_* \approx 18$, and a chemical guiding pattern extends this favorable parameter window to large values of incompatibility.

To test this prediction of mean-field theory by our particle simulations we quench the two structures that formed persistent defects on guiding patterns with 2×density multiplication on a neutral background (see Fig. 3) at $t = 1.3 \cdot 10^6$ SMC $\approx 145\tau$ from $\chi N = 30$ to 20. Although there is a significant mismatch of -6% between the half period of the sparse guiding pattern and the bulk lamellar spacing at $\chi N = 20$, defects readily annihilated within 30000 SMC $\approx 3.3\tau$. Reestablishing the original incompatibility $\chi N = 30$ at $t = 1.33 \cdot 10^6$ SMC we observe that the segregation between A and B-domains increases and the line-edge roughness of the AB interfaces decreases but no defects are formed.

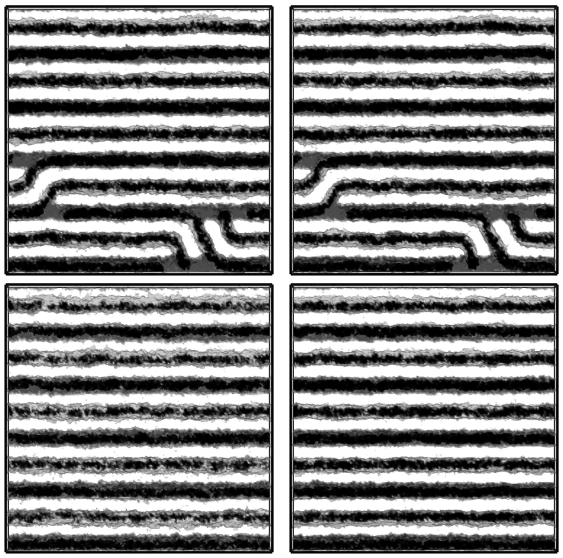

Figure 8. Top-down images of the ordering on a L/S guiding pattern with 2×density multiplication. The guiding pattern consists of A-attractive lines with $W/L_0 = 1/2$ and $\Lambda N = 2$ on a neutral background, $\Lambda_s N = 0$. The system was quenched from a disordered state to $\chi N = 30$ far below the ODT, and subsequently annealed for $1.3 \cdot 10^6$ SMC. This long annealing did not result in defect free-ordering. Then the system was quenched closer to the ODT, $\chi N = 30 \to 20$. Annealing for only $3 \cdot 10^4$ SMC in this DSA-favorable parameter window removed all defects. After increasing the incompatibility back to its original value $\chi N = 30$ t $t = 1.33 \cdot 10^6$ SMC the structure remains defect-free. The different panels present snapshots at $t = 5 \cdot 10^5, 1.3 \cdot 10^6, 1.33 \cdot 10^6$, and $1.5 \cdot 10^6$ SMC.

4. Summary and discussion

Using a soft, coarse-grained model of block copolymer melts in conjunction with efficient, parallel simulation techniques we have studied the kinetics of structure formation of lamella-forming copolymer films on chemical guiding patterns. Both the replication of the guiding pattern and two-fold density multiplication have been investigated in the limit of perfect commensurability between the bulk lamellar structure and the L/S guiding pattern. Defect-free pattern replication is driven by the pattern-directed spinodal self-assembly. It is robust and only requires a time, τ, that is comparable to the longest time of conformational relaxation. Density multiplication, in turn, requires significantly longer annealing times at $\chi N = 30$, and it sensitively depends on the DSA process parameters. In our simulation study we have illustrated the dependence on incompatibility and strength of the surface interactions. In agreement with experiments and previous simulations that focused on the equilibrium properties [14, 15], we observe that sparse guiding patterns of A-attractive lines with a background that is weakly attractive to the other species, B, are preferable to neutral backgrounds. Our simulations indicate that such a weak background preference results in a more symmetric structure at the end of the initial pattern-directed spinodal self-assembly (i.e. after a time τ), and thereby reduces the number of metastable, persistent defects. Our simulations also highlight the benefits of performing the DSA process in the vicinity of the order-disorder transition and thereby corroborate our recent self-consistent field study on defect annihilation mechanisms [21].

The tailoring of the time dependence of thermodynamic process variables ("process-directed self-assembly" [45]) – here, the incompatibility χN – opens additional opportunities for directing the structure formation in block copolymer systems and has also been found to be a promising strategy for fabricating bicontinuous network structures [46]. This strategy relies on the observation that the free-energy landscape changes with the external thermodynamic process conditions and that pathways of collective structure changes sensitively depend on the structure of the complex free-energy landscape.

In an experiment the incompatibility can be changed by temperature if the Flory-Huggins parameter χ exhibits a significant temperature dependence or by adding a co-solvent. Solvent tempering is a common strategy for defect removal. In the simplest case, the solvent uniformly dilutes the repulsive interactions between unlike segment species [47, 48]. This results in a

reduction of the effective incompatibility and, additionally, speeds up the segmental dynamics ("plasticizing effect") and may also alter the equilibrium period of the microphase-separated structure. In an experiment it may be difficult to disentangle these different effect, and our simulation study highlights the specific role of the free-energy landscape.

Acknowledgments
It is a great pleasure to thank Juan J. de Pablo, Paul F. Nealey, and Mark P. Stoykovich for stimulating discussions and fruitful collaborations. The authors wish to acknowledge financial support from the European Union FP7 under grant agreement No.619793 CoLiSA.MMP (Computational Lithography for Directed Self-Assembly: Materials, Models, and Processes) and the Deutsche Forschungsgemeinschaft under grant Mu1674/11. The simulations have been enabled by the generous access to the computing facilities at the GWDG Göttingen, the HLRN Hannover/Berlin and the Jülich Supercomputing center.

References

[1] Leibler L 1980 *Macromolecules* **13** 1602–1617
[2] Fredrickson G H and Bates F S 1996 *Ann. Rev. Mater. Sci.* **26** 501–550
[3] Stoykovich M P and Nealey P F 2006 *materials today* **9** 20–29
[4] Bita I, Yang J K W, Jung Y S, Ross C A, Thomas E L and Berggren K K 2008 *Science* **321** 939–943
[5] Hawker C J and Russell T P 2005 *MRS Bulletin* **30** 952–966
[6] Bang J, Jeong U, Ryu D Y, Russell T P and Hawker C J 2009 *Advanced Materials* **21** 4769–4792
[7] Bates C M, Maher M J, Janes D W, Ellison C J and Willson C G 2014 *Macromolecules* **47** 2–12
[8] Kim S O, Solak H H, Stoykovich M P, Ferrier N J, de Pablo J J and Nealey P F 2003 *Nature* **424** 411–414
[9] Edwards E W, Stoykovich M P, Müller M, Solak H H, de Pablo J J and Nealey P F 2005 *J. Polym. Sci. B: Polymer Physics* **43** 3444–3459
[10] Edwards E W, Müller M, Stoykovich M P, Solak H H, de Pablo J J and Nealey P F 2007 *Macromolecules* **40** 90–96
[11] Daoulas K C, Müller M, Stoykovich M P, Kang H, de Pablo J J and Nealey P F 2008 *Langmuir* **24** 1284–1295
[12] Stoykovich M P, Daoulas K C, Müller M, Kang H M, de Pablo J J and Nealey P F 2010 *Macromolecules* **43** 2334–2342
[13] Ruiz R, Kang H M, Detcheverry F A, Dobisz E, Kercher D S, Albrecht T R, de Pablo J J and Nealey P F 2008 *Science* **321** 936–939
[14] Detcheverry F A, Liu G L, Nealey P F and de Pablo J J 2010 *Macromolecules* **43** 3446–3454
[15] Liu C C, Ramirez-Hernandez A, Han E, Craig G S W, Tada Y, Yoshida H, Kang H, Ji S, Gopalan P, de Pablo J J and Nealey P F 2013 *Macromolecules* **46** 1415–1424
[16] Li W H, Müller M 2015 *Annu. Rev. Chem. Biomol. Eng* in press
[17] Jeong S-J, Kim J Y, Kim B H, Moon H-S and Kim S O 2013 *Materials Today* **16** 468–476
[18] Nagpal U, Müller M, Nealey P F and de Pablo J J 2012 *ACS Macro Letters* **1** 418–422
[19] Duque D, Katsov K and Schick M 2002 *J. Chem. Phys.* **117** 10315–10320
[20] Müller M, Daoulas K C and Norizoe Y 2009 *Phys. Chem. Chem. Phys.* **11** 2087
[21] Li W H, Nealey P F, de Pablo J J and Müller M 2014 *Phys. Rev. Lett.* **113** 168301
[22] Daoulas K C, Müller M, de Pablo J J, Nealey P F and Smith G D 2006 *Soft Matter* **2** 573–583
[23] Müller M 2011 *J. Stat. Phys.* **145** 967–1016
[24] Detcheverry F A, Pike D Q, Nealey P F, Müller M and de Pablo J J 2009 *Phys. Rev. Lett.* **102** 197801
[25] Müller M, Steinmüller B, Daoulas K C, Ramirez-Hernandez A and de Pablo J J 2011 *Phys. Chem. Chem. Phys.* **13** 10491–10502
[26] Geisinger T, Müller M and Binder K 1999 *J. Chem. Phys.* **111** 5241–5250
[27] Müller M 2012 *Phys. Rev. Lett.* **109** 087801
[28] Rossky P J, Doll J D and Friedman H L 1978 *J. Chem. Phys.* **69** 4628–4633
[29] Daoulas K C and Müller M 2006 *J. Chem. Phys.* **125** 184904
[30] Müller M and Daoulas K C 2008 *J. Chem. Phys.* **129** 499–503
[31] Ramirez-Hernandez A, Müller M and de Pablo J J 2013 *Soft Matter* **9** 2030–2036
[32] Tuckerman M, Berne B and Martyna G 1992 *J. Chem. Phys.* **97** 1990
[33] Müller M and Daoulas K C 2011 *Phys. Rev. Lett.* **107** 227801
[34] deGennes P G 1979 *Scaling concepts in polymer physics* (Cornell University Press, Ithaca)
[35] Hohenberg P C and Halperin B I 1977 *Rev. Mod. Phys.* **49** 435–479

[36] Cross M C and Hohenberg P C 1993 *Rev. Mod. Phys.* **65** 851–1112
[37] Binder K 1983 *J. Chem. Phys.* **79** 6387–6409
[38] Reister E, Müller M and Binder K 2001 *Phys. Rev. E* **64** 041804
[39] Reister E and Müller M 2003 *J. Chem. Phys.* **118** 8476–8488
[40] Peach M and Koehler J S 1950 *Phys. Rev.* **80** 436–439
[41] Pershan P S 1974 *J. Appl. Phys.* **45** 1590–1604
[42] Hahm J and Sibener S J 2001 *J. Chem. Phys.* **114** 4730–4740
[43] Harrison C, Adamson D H, Cheng Z, Sebastian J M, Sethuraman S, Huse D A, Register R A and Chaikin P M 2000 *Science* **290** 1558–1560
[44] Harrison C, Cheng Z, Sethuraman S, Huse D A and Chaikin P M 2002 *Phys. Rev. E* **66** 011706
[45] Müller M and de Pablo J J 2013 *Annu. Rev. Mater. Sci.* **43** 1–34
[46] Müller M and Sun D W 2013 *Phys. Rev. Lett.* **111** 267801
[47] Naughton J R and Matsen M W 2002 *Macromolecules* **35** 5688–5696
[48] Rudov A A, Patyukova E S, Neratova I V, Khalatur P G, Posselt D, Papadakis C M and Potemkin I I 2013 *Macromolecules* **46** 5786–5795